

Experimental and Computational Investigation of Structural Integrity of Dissimilar Metal Weld Between Ferritic and Austenitic Steel



R. SANTOSH, G. DAS, S. KUMAR, P.K. SINGH, and M. GHOSH

The structural integrity of dissimilar metal welded (DMW) joint consisting of low-alloy steel and 304LN austenitic stainless steel was examined by evaluating mechanical properties and metallurgical characteristics. INCONEL 82 and 182 were used as buttering and filler materials, respectively. Experimental findings were substantiated through thermomechanical simulation of the weld. During simulation, the effect of thermal state and stress distribution was pondered based on the real-time nuclear power plant environment. The simulation results were co-related with mechanical and microstructural characteristics. Material properties were varied significantly at different fusion boundaries across the weld line and associated with complex microstructure. During *in-situ* deformation testing in a scanning electron microscope, failure occurred through the buttering material. This indicated that microstructure and material properties synergistically contributed to altering the strength of DMW joints. Simulation results also depicted that the stress was maximum within the buttering material and made its weakest zone across the welded joint during service exposure. Various factors for the failure of dissimilar metal weld were analyzed. It was found that the use of IN 82 alloy as the buttering material provided a significant improvement in the joint strength and became a promising material for the fabrication of DMW joint.

<https://doi.org/10.1007/s11661-018-4554-y>

© The Minerals, Metals & Materials Society and ASM International 2018

I. INTRODUCTION

IN nuclear power plants, the primary water circuit of pressurized heavy water reactors (PHWRs) consists of dissimilar metal welded (DMW) joint. The two materials in DMW joints are low-alloy steel and 304 austenitic stainless steel.^[1] ASTM S508 Grade 3 Class I low-alloy ferritic steel (low-alloy steel) is used as the nozzle piping material for nuclear pressure vessels, steam generators, and pressurizers due to its high toughness and low cost. The connecting primary pipelines are made with SA312 type 304LN austenitic stainless steel (304LN SS) owing to its adequate corrosion resistance and satisfactory strength.^[2] The complex microstructures and chemical changes across the fusion boundary of this DMW joint result in frequent failure during service. Several

weld-related failures, such as leaks and breakages, were reported earlier.^[3] The major reasons for this kind of degeneration were a disparity in mechanical properties, complexities in the metallurgical phenomenon, and carbon diffusion across the interface. Other factors, such as the migration of alloying elements through the fusion zone, variation in the weld metal composition due to the change in base metal dilution, the formation of narrow carbon-depleted zone, and phase transformation near the fusion boundary, were discussed in detail.^[4] To overcome the limitations of austenitic stainless steel as welding consumable, the use of Ni-base alloys was attempted for fabricating DMW joints. Ni-base alloys exhibit better compatibility to base metals with respect to stainless steel.^[5-9] Further, they play a major role in restricting the carbon diffusion through the fusion boundary from the low alloy to the austenitic steel side and have a coefficient of thermal expansion between ferrite and austenite.^[10-15]

In this respect, low-alloy steel was joined with 316 SS using INCONEL* 82 buttering material and IN 182

R. SANTOSH is with the Department of Mechanical and Manufacturing Engineering, Manipal Institute of Technology, Manipal 576104, India. G. DAS and M. GHOSH are with the Materials Science & Technology Division, CSIR-National Metallurgical Laboratory, Jamshedpur 831007, India. Contact email: ghosh_mnk@yahoo.com S. KUMAR and P.K. SINGH are with the Reactor Safety Division, Bhabha Atomic Research Centre, Mumbai 400085, India.

Manuscript submitted July 10, 2017.

Article published online March 20, 2018

*INCONEL is a trademark of International Nickel Co., INC., USA.

filler material.^[1] The variation of mechanical properties was examined by tensile and microhardness tests.

Tensile specimens were drawn from various locations (top, middle, and bottom) of the welded joint. It was found that the tensile properties and fracture characteristics were varied across the fusion boundary of low-alloy steel and buttering material. The results represent that within INCONEL fusion weld, the yield strength (YS) and ultimate tensile strength (UTS) were about 50 to 70 MPa higher at the bottom compared to the top region. Fractography revealed that failure was through ductile dimple fracture and shear stretch mode at the bottom and top of the weld joint, respectively. In a different endeavor, four types of weld metal (316 SS, 16-8-2 SS, IN 182, and IN 82) were used for joining Alloy 800 low-carbon steel with 316LN SS.^[7] A comparative evaluation was done based on hot cracking tests and mechanical properties estimation. Failure was in the fusion zone for the joints with 316 SS and 16-8-2 SS weld metals. Cracking was at the parent material for joints with IN 182 and IN 82 weld metals. It was also established that the use of Ni-base alloys contributed significantly to an increase in UTS and YS of the joints. The microstructure and mechanical properties of the dissimilar welded joint between SA508 Grade 1a ferritic steel and F316 SS with Alloy 82/182 filler material were investigated by Kim *et al.*^[8] The results of tensile testing revealed that the material properties varied significantly at different zones. Moreover, the change was significant near the HAZs of F316 SS and SA508 Gr.1a ferritic steel due to dislocation-induced strain hardening and phase transformation during welding, respectively.

Direct measurement and study of the stress profile, temperature distribution, heat generation, and deformation across the DMW joint during service exploitation are difficult. Therefore, for a reliable integrity analysis, simulation of these DMW joints subjected to the real-time operating conditions is beneficial to provide a clear insight into the condition of the material during service. To understand the phenomena, ANSYS-based simulations were attempted earlier. Ramamurthy^[16] and Chandraptla and Belegundu^[17] formulated the basic finite-element models for welding, which involved structural and heat-transfer characteristics. From this basic elemental approach, one-dimensional, two-dimensional (2-D), and three-dimensional (3-D) models could be developed for simulations of both steady-state and transient heat-transfer conditions. The simulation accuracy was based on linear and quadratic shape functions, which were considered during modeling. In a different study, a complete stress analysis and temperature distribution of welds were computed using a nonlinear transient finite-element heat flow program by Goldak *et al.*^[18] A simulation based on the finite-element method (FEM) was developed for examining the effect of weld heat sources on heat flux. Ellipsoidal and double ellipsoidal geometries of Gaussian distribution of power density in the weld heat source were considered for the mathematical model. The model was designed in such a way that both shallow penetration arc welding and the deeper penetration laser/electron beam welding heat source could be considered under the same spectrum. The results illustrated that the computed temperature and stress distributions were in good

agreement with the measured values for both shallow and deep penetration welding processes. Akella *et al.*^[19] developed Gaussian distribution models for laser, electron, and plasma welding applications. They investigated laser beam joining of similar material using constant heat flux with a Gaussian beam source. A 3-D weld model was used for analysis, which considered frustum, ellipsoid, and Gaussian heat modes.

Sahin *et al.*^[20] carried out a simulation of the DMW joint consisting of copper and steel. They used a 2-D approach with FORTRAN.** Residual and thermal

**Fortran is a trademark of Compaq Information Technologies Group, L.P., USA.

stress distributions across the transverse direction of the dissimilar weld joint were investigated. The results showed that thermal stress was tensile along the heat-affected zone (HAZ) and compressive away from the HAZ. It was also inferred that the thermal effect was responsible for creating residual stress in the transverse direction of the weld joint. Xu and co-workers carried out finite-element simulation on the DMW joint between austenitic electrode A302 and Ni-base electrode IN 182 as weld metals using ABAQUS 6.5.^[21] Both the temperature and stress field were considered as governing parameters, as variation in any one field would vary the mechanical properties of the welded joint. The simulation results described that with the use of IN 182, thermal stress distribution became declining in nature. To achieve more reliability and better durability further, different types of alloys were also used for this type of transition joint.^[22] One of the recent alloys in this respect was IN 82.^[23,24]

Residual stress was evaluated for the welded joint between ferritic and austenitic steel using the X-ray diffraction (XRD) technique.^[24] IN 82 was used as buttering and filler metal. The residual stress measurement along the circumferential and axial directions revealed a substantial reduction in the stress level at the HAZ.

Even with the use of Ni-base welding consumables, a number of failures have also been reported in the recent past for the transition joint between ferritic and austenitic steels.^[25-27] Therefore, it is necessary to identify major factors contributing to the failure of these DMW joints. Moreover, from the preceding discussion, it was obvious that most of the numerical analysis included residual and thermal stresses that were generated during fabrication of the joints. A single parameter (effect of temperature or stress) was considered as the contributing factor for failure in an isolated fashion. However, thermal stress generation and its distribution across the joint during real-time operating conditions in nuclear power plants are important to evaluate the stress generation's realistic structural heterogeneity and lifespan. For the same, both the temperature and stress effects are considered during simulation analysis. These two features become responsible for gradual structural degeneration and act as an

indicative parameter to identify the vulnerable location of the failure.

With the change in welding consumable during the experimental investigation, qualitative and quantitative variations are expected in microstructural features, mechanical properties, and stress distribution. To identify the preferable buttering material for joining low-alloy steel and 304LN SS with better structural stability/reliability and joint strength, welded joints were produced with IN 182 consumables previously.^[22,31] In the present study, IN 82 buttering material was used for welding the same base alloys. This replacement indicated a radical change in structural characteristics and mechanical properties of the welded assembly with respect to other transition joints made with different consumables. To explore the reason, 3-D FEM-based thermomechanical simulation was done considering thermal and mechanical stress distribution apart from mechanical and structural characterization. This attempt provides a clear understanding of the effect of different buttering materials for joining ferritic to stainless steel and selecting a preferable welding consumable for producing welds with improved reliability and mechanical properties.

II. EXPERIMENTAL TECHNIQUE

SA508 Gr.3 Cl.I ferritic steel and SA312 type 304LN austenitic stainless steel were used as parent materials for welding. The buttering and filler materials were IN 82 and IN 182, respectively. Layerwise buttering with an ultimate total thickness of ~ 5 mm was carried out on the low-alloy steel side, followed by postweld heat treatment (PWHT) at ~ 923 K (650 °C) for 90 minutes to relieve stress. The gas tungsten arc welding (GTAW) technique was employed for both buttering metal (IN 82) and filler metal (IN 182). The chemical composition of alloys is shown in Table I. Spark emission spectrometry was used to determine the bulk chemical composition of low-alloy steel and 304LN SS using a rectangular block of cross section ~ 20 mm². The block was initially polished, cleaned in acetone, and exposed to an electrode for spark creation. The readings were directly obtained from the viewing screen. For IN 82 and IN 182 alloys, the composition was determined using an inductively coupled plasma spectrometer after dissolving the alloys in acidic solution. Further, a LECO[†] gas analyzer was used to

[†]LECO is a trademark of LECO Corporation, St. Joseph, MI.

quantify the concentration of carbon, sulfur, and nitrogen in all alloys using fine turnings. The schematic of the weld joint is shown in Figure 1(a). Details of the welding technique are discussed elsewhere.^[28,29]

From the welded joint, sampling was carried out through the middle of the transverse section and a conventional metallographic technique was followed for specimen preparation. The microstructural observation was done on various locations of the welded assembly

(Figure 1(b)). Nital and Glycergia were used for etching low-alloy steel and buttering material-filler metal-304LN SS, respectively. The microstructural examination was performed using optical and scanning electron microscopes for revealing structural details near the fusion boundaries. Quantification and statistical analysis of microstructural features were done with the help of image analysis software.

Microhardness was measured across fusion boundaries at a depth of ~ 10 mm from the top edge of the weld. A 50-g load was applied during measurement, and the interval was ~ 1.0 mm between two successive indents. For identification of the sharp change near fusion boundaries, the interval was reduced to ~ 0.3 mm. An XRD study was done close to the fusion boundary between the low-alloy steel and buttering material to identify the reaction products. During experimentation, the scanning span was 25 to 100 deg, the step size was ~ 0.02 deg/s, and the residence time was ~ 2 seconds. Sampling was carried out by cutting a section parallel to the fusion boundary by electric discharge machining. The cut surface was within the low-alloy steel and ~ 2.0 mm away from the fusion line between low-alloy steel and buttering material. The surface was polished and cleaned by sonication using acetone. XRD was performed on that surface. The preceding processes were repeated after removing layer after layer to ultimately reach a buttering material.

The mechanical properties of the welded joint were determined using *in-situ* tensile testing equipment, attached with a scanning electron microscope (SEM). Sampling was carried out close to the center of the transverse section (~ 10 mm from the top edge of the welded specimen), as shown in Figure 2(a), through a low-alloy steel-IN 82 buttering material interface. Most of the premature failure/disbonding of the welded joint occurred predominantly from that location.^[1,7,30] The schematic diagram of the machined *in-situ* tensile specimen is shown in Figure 2(b). Experiments were executed on a stage with a 2-kN load cell. Prior to testing, one of the surfaces of the flat tensile specimen was polished to obtain a mirror finish. During testing, the crosshead speed was at ~ 0.05 mm/min. Secondary electron (SE) images were captured at regular intervals to record the structural changes over gage length, crack initiation, and failure path during deformation. After testing, the fracture surfaces were examined in an SEM.

III. CONCEPT OF NUMERICAL MODEL

A. Governing Equations and Boundary Conditions

Time- and temperature-dependent properties of materials play an important role in the structural stability of the DMW joints. Therefore, thermomechanical simulation of the DMW joint was carried out to provide further perception about its behavior with IN 82 as the buttering material during real-time service condition. An FEM-based thermomechanical simulation was attempted to predict the thermal effect and stress distribution across the joint (Figure 3).

Table I. Chemical Composition of Base Metals and Welding Consumables

Alloys	Concentration of Alloying Elements (Weight Percent)											
	C	Mn	P	S	Si	Ni	Cr	Mo	Cu	Al	Nb	Fe
Low-alloy steel	0.20	1.2	0.01	0.001	0.001	0.80	0.20	0.50	0.03	0.04	—	bal
304LN SS	0.03	2.0	0.05	0.03	1.0	8.0	18.0	—	—	—	—	bal
IN 82	0.10	2.5	0.03	0.02	0.5	bal	18.0	—	0.50	—	2.0	3.0
IN 182	0.10	5.0	0.03	0.02	1.0	bal	13.0	—	0.50	—	1.0	10.0

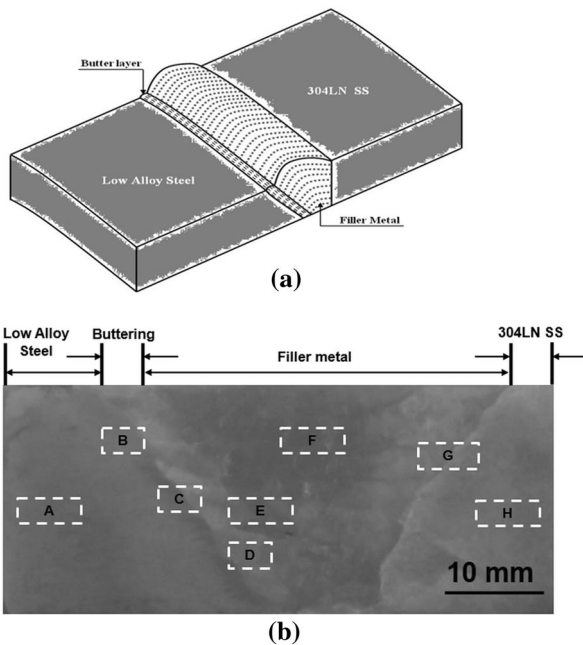


Fig. 1—DMW joint (a) schematic diagram and (b) cross-sectional macrograph showing locations of microstructural investigation.

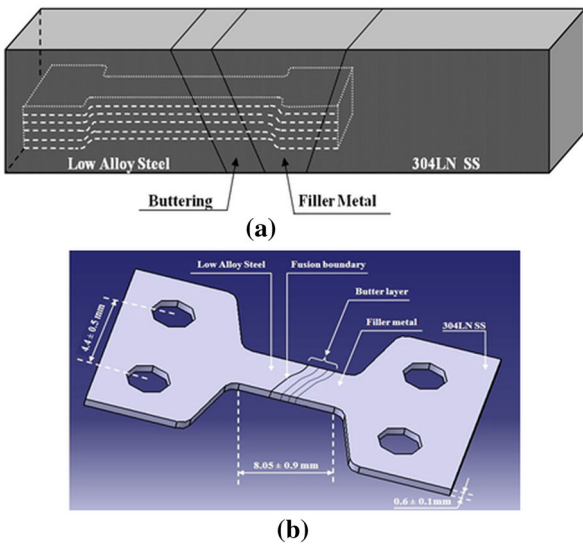


Fig. 2—Tensile specimen from DMW joint (a) sampling location for the tensile specimen and (b) miniature machined tensile sample (not to scale).

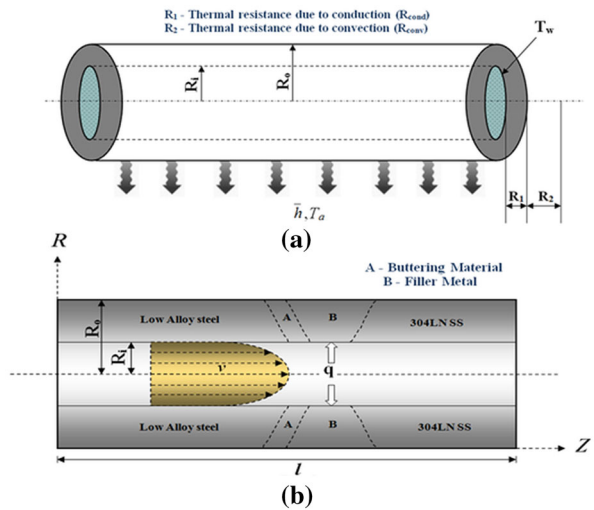


Fig. 3—Schematics of DMW pipe showing (a) radial heat flow with resistance against it and (b) coordinates.

Generally, three types of heat transfer take place when steam flows through the DMW joint, namely, conduction, convection, and radiation. For the present situation, the effect of radiation is minimal. Therefore, assuming unidirectional steady-state heat transfer without heat generation, the conduction equation, the rate of heat conduction, the overall heat-transfer rate, and the steam flow energy balance remained the same as formulated earlier.^[31] At the solid-steam interface, the specific heat flux and heat conduction equations for steady-state analysis were determined. In that case, boundary conditions, such as the radial velocity gradient with no slip conditions, the flow of steam with uniform temperature, the minimum heat-transfer rate at the outer surface of the DMW pipe compared to the inner surface, and the uniform heat flux along the radius and length of the pipe were taken into consideration. The DMW pipe was considered as a hollow cylinder. Thermal and effective stresses on the DMW pipe were determined from thermoelastic formulae and von Mises theory, respectively, the cogitating modulus of elasticity, Poisson's ratio, and the thermal expansion ratio of the alloys used in the joint.^[31]

B. Description of the Model

Thermomechanical simulation of the DMW joint was performed using CATIA and FEM for the given operating conditions. During analysis, the conservation

of mass, momentum, and energy was taken into deliberation. The major objective of the numerical analysis was to identify and analyze the areas within the weld, prone to accumulation of thermal stress under an operating temperature of ~ 561 K (288 °C).^[32]

From the available information, the dimensions of the DMW pipe were $D \sim 324$ mm with wall thickness ~ 27 mm.^[32] It was assumed that steam flowed with uniform steady-state velocity through the pipe. The mechanical properties of different materials used in the present study are listed in Table II.^[7,31] The thermomechanical properties of materials used in the present analysis are shown in Figure 4.^[32–35] Design and meshing were

carried out based on the accuracy and efficiency of the computation.

IV. RESULTS AND DISCUSSION

A. Microstructure of Base Metal and Weld Metals

The microstructures of low-alloy steel and 304LN SS (locations A and H) are shown in Figures 5(a) and (b), respectively. The microstructure of low-alloy steel consisted of tempered martensite, while that of 304LN SS contained polygonal austenitic grains with annealing twins. The microstructure at these two locations did not vary significantly due to the effect of heat flow during welding and the PWHT process.

The microstructures of the buttering material IN 82 and filler metal IN 182 (D and F in Figure 1(b)) are shown in Figures 6(a) and (b), respectively. The buttering material revealed the signature of dendritic solidification. It consisted of austenite with transversely developed columnar crystals. Predominant austenitic/ferritic (AF) and occasional ferritic/austenitic (FA) solidification modes were observed adjacent to the LAS-IN 82 fusion boundary within the buttering material (Figure 6(a)). Further, the coalescence of

Table II. Mechanical Properties of Base Metals and Welding Consumables

Alloys	0.2 Pct YS (MPa)	UTS (MPa)	Breaking Strain (Pct)
Low-alloy steel	250 ± 5	638 ± 8	20 ± 1
304LN SS	205 ± 3	515 ± 6	40 ± 2
IN 82	333 ± 5	630 ± 6	36 ± 2
IN 182	312 ± 4	613 ± 6	30 ± 2

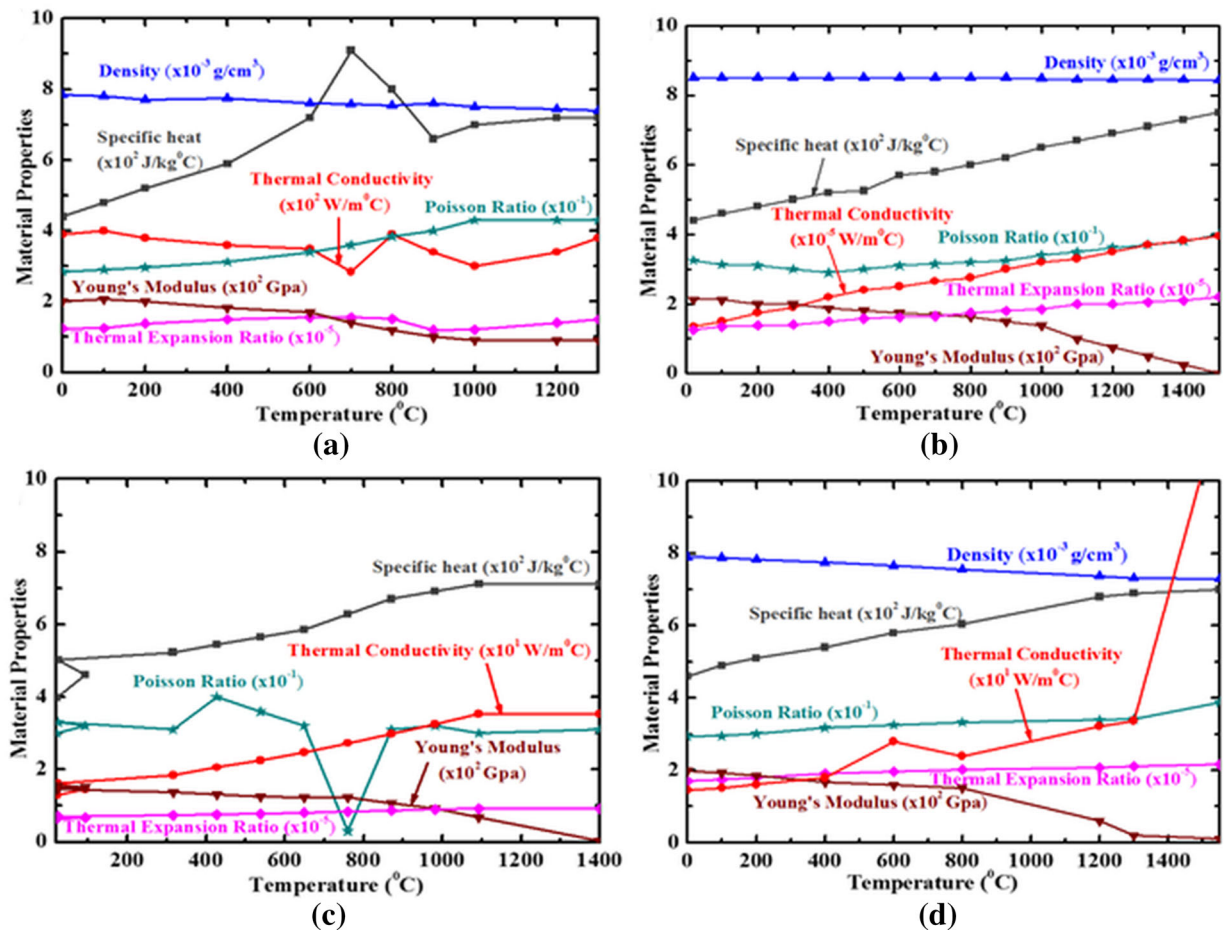


Fig. 4—Temperature-dependent properties of (a) LAS, (b) IN 82, (c) IN 182, and (d) 304LN SS (reprinted from Ref. [31]).

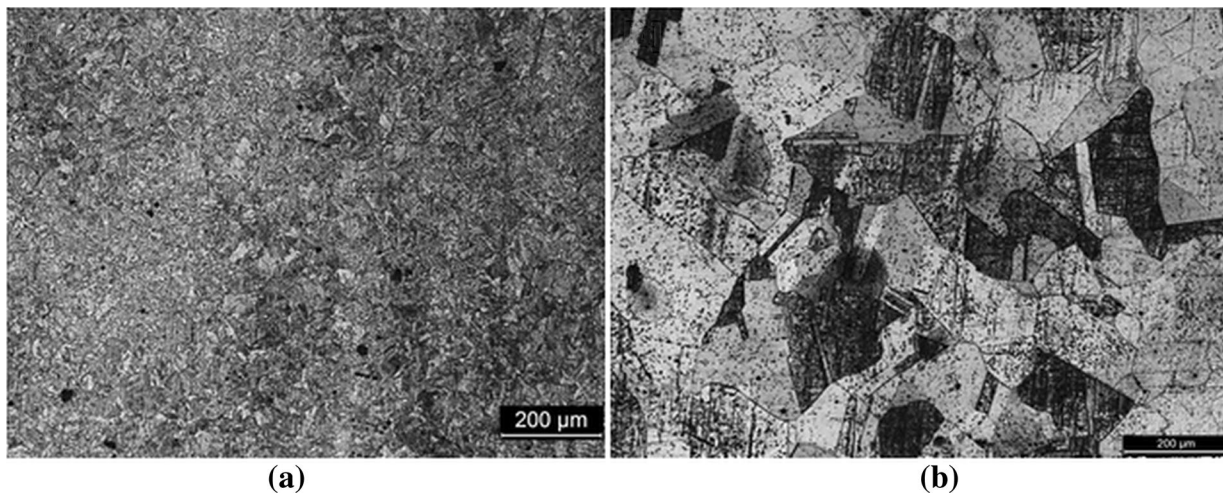


Fig. 5—Microstructure of base metals: (a) LAS and (b) 304LN SS.

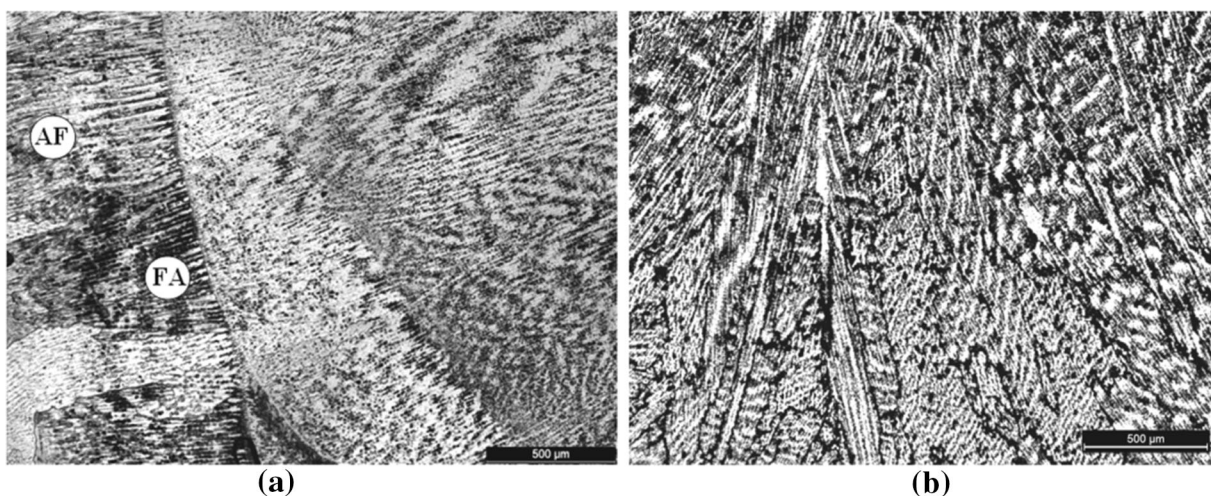


Fig. 6—Optical images of solidified (a) buttering material IN 82 and (b) filler metal IN 182.

subgrains resulted in extensive grain boundary migration within the IN 82 austenitic alloy away from the fusion boundary.^[36] The filler metal IN 182 exhibited longitudinal columnar growth of austenite along with solidification boundaries (Figure 6(b)). The difference in the columnar crystal orientations could be attributed to the different directions of cooling after welding.^[9] Ni and Cr were the major chemical species in filler metal, and their tendency of segregation was very small.^[36] The driving force was low during solidification; therefore, cellular morphology was developed within the filler metal along with the appearance of secondary phases, globular precipitates, and oxide inclusions.^[6]

B. Microstructure at Fusion Boundaries

Heat flow and diffusion of the elements during and after welding resulted in a complex microstructure at different fusion boundaries of the DMW joint. Microstructures at the fusion boundary between the low-alloy steel and buttering material (locations B and C

of Figure 1(b)) are shown in Figures 7(a) and (b). The microstructure of low-alloy steel after welding could be divided into three regions: region 1 (L1), region 2 (L2), and region 3 (L3) (Figure 7(a)). L1 corresponded to the unchanged structure of low-alloy steel. L2 exhibited fine polygonal ferrite grains containing a dispersion of cementite. L3, which was close to the fusion boundary, revealed the ferrite-pearlite mixture. The widths of L2 and L3 were found to be ~ 260 to $1140 \mu\text{m}$ and ~ 19 to $74 \mu\text{m}$, respectively. Ferrite grains in L3 were coarser than in L2. The widths of these regions and the ferrite grain size depended on the buttering material and welding technique.^[22] The concentration gradient was responsible for carbon migration from L3 to the buttering material during welding and PWHT.^[5] The depletion of carbon at L3 resulted in reduction of the second-phase area fraction. Therefore, ferrite grain growth was facilitated. The grain size of this region was $\sim 12 \mu\text{m}$. In region L2, the original base material microstructure disappeared due to the effect of heat dissipation after welding and during PWHT. Martensite

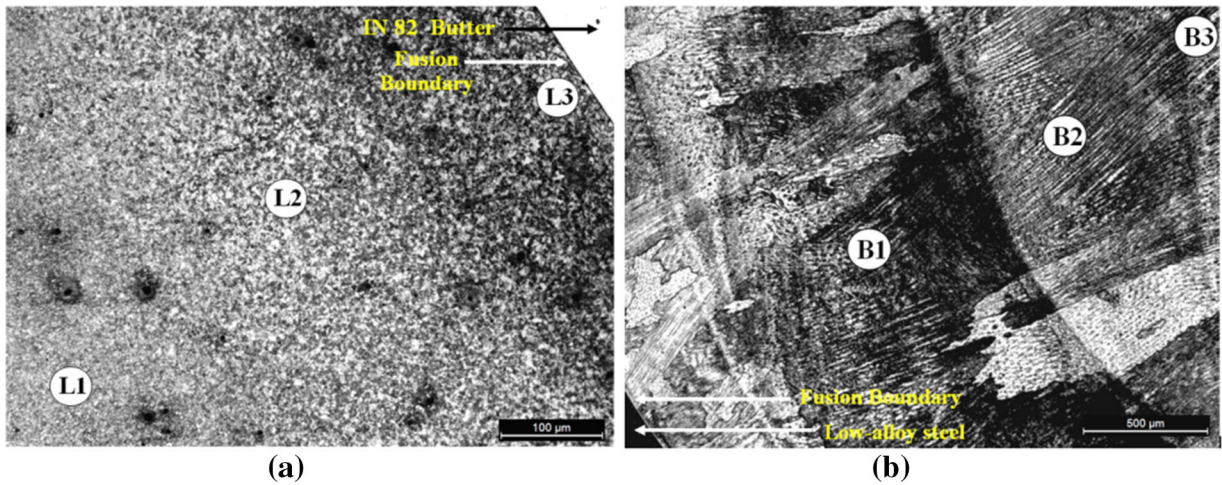


Fig. 7—Microstructure at LAS-IN 82 interface region: (a) LAS side corresponding to position “A to B” and (b) IN 82 side corresponding to position “C to D.”

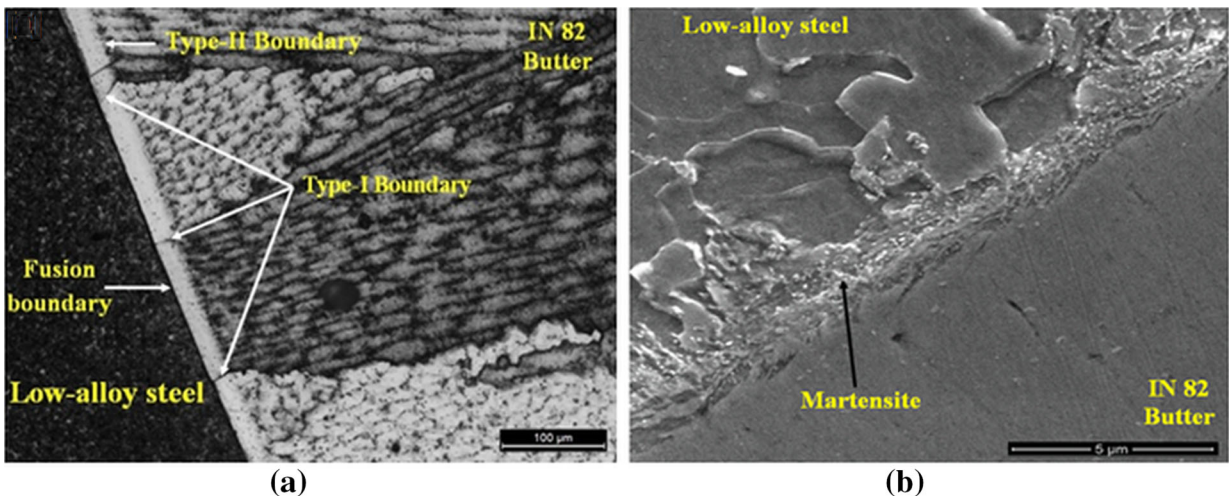


Fig. 8—Microstructure adjacent to LAS-IN 82 fusion boundary corresponding to position “C” showing (a) type-I and II boundaries and (b) lath martensite.

became tempered and transformed to fine ferrite and pearlite phase aggregate. Across the buttering material from the fusion boundary, three layers were identified as B1, B2, and B3, respectively (Figure 7(b)). The total width of these three regions was ~ 3000 to 4000 μm . Apart from the presence of AF and occasional FA modes of solidification in the buttering material, a coalition of subgrains and extensive grain boundary migration was found within the solidification structure away from the fusion boundary.^[36]

The complex microstructure was identified adjacent to the fusion boundary of low-alloy steel and IN 82 (location C of Figure 1(b)). Two different boundaries, namely, types I and II, were identified at this location (Figure 8(a)). The type-I boundary was perpendicular, and the type-II boundary was parallel to the fusion boundary. The type-I boundary originated from the fusion boundary when the columnar grain growth of low-alloy steel took place in the buttering material and

became nearly perpendicular to the fusion boundary.^[36,37] When low-alloy steel became ferritic and IN 82 was austenitic near the melting point, the normal epitaxial growth was suppressed and the heterogeneous nucleation of fcc buttering material resulted in the formation of the type-II boundary parallel to the fusion boundary. This type-II boundary was considered as an inherent high-energy boundary.^[4–6] The location of this boundary was near ~ 18 to 36 μm away from the fusion boundary and was within the buttering material.

At the same interface close to the fusion boundary, as shown in Figure 8(b), the blocky island of fine lath martensite was present. Low-alloy steel contained higher carbon compared to IN 82. During fabrication, carbon migration occurred from low-alloy steel to IN 82, as mentioned earlier.^[4] IN 82 contained a much higher amount of Cr than low-alloy steel. This also encouraged carbon migration during PWHT.^[11] The carbon-enriched region transformed to martensite during cooling.

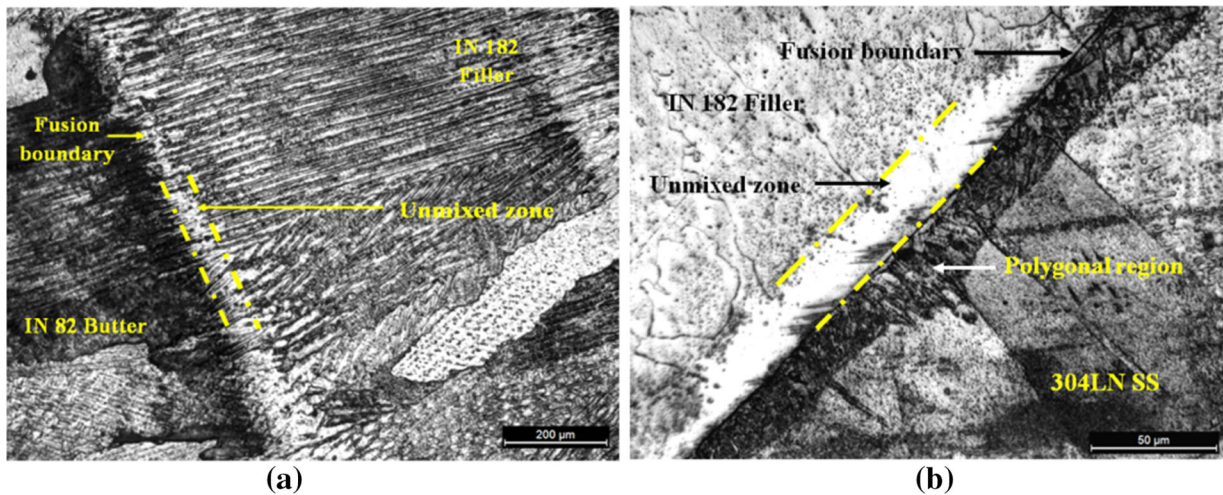


Fig. 9—Optical micrographs near the interface between (a) IN 82-IN 182 and (b) IN 182-304LN SS.

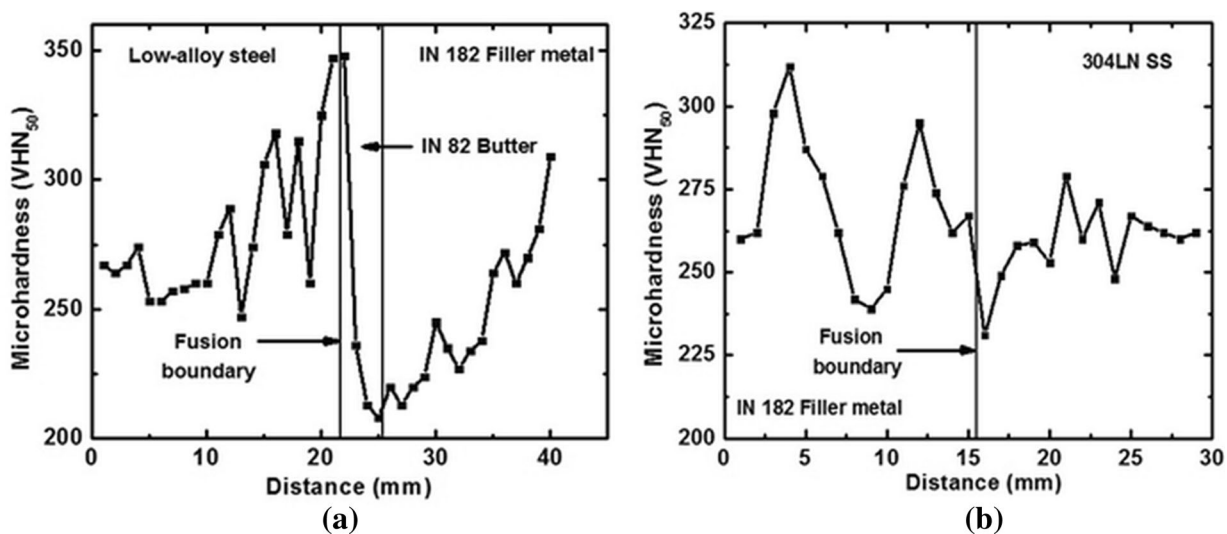


Fig. 10—Microhardness profiles across (a) LAS-IN 82 and (b) IN 182-304 LN SS interface regions of the DMW joint.

Martensite is one of the hardest phases, so hardness in this region was increased (Figure 10(a)). During PWHT, initially, the previously formed martensite (during welding) was tempered, and at a later stage, further migration of carbon formed fresh lath martensite. The synergistic effect of these two mechanisms resulted in variation of microhardness of this region (Figure 10(a)). Evolution of phases near the fusion boundary between LAS-IN82 buttering material was confirmed by XRD study (Figure 11). The distribution of narrow martensitic cluster was discontinuous in nature and its thickness was found to be ~ 2 to $10 \mu\text{m}$. Previous studies revealed that the thicknesses of martensite with the use of 309L SS and IN 182 buttering materials were ~ 7 to $16 \mu\text{m}$ and ~ 8 to $11 \mu\text{m}$, respectively, during joining of the same parent materials.^[22,23] Thus, the use of IN 82 buttering material significantly reduced the width of martensite compared to 309L SS and IN 182 buttering

materials for joining low-alloy steel and 304LN SS. The reduction in the width of the martensitic layer could be attributed to the limited diffusion of carbon in IN 82 when compared to that of 309L SS and IN 182.^[4,22] IN 82 contained a substantially higher quantity of Cr with respect to 309L SS and IN 182. As the concentration of chromium was increased, carbon diffusion through austenite became sluggish. The slow carbon diffusion could be attributed to the reduction of its activity within austenite in the presence of a substantial quantity of carbide former.^[38] At the same time, the increment in chromium content in IN 82 reduced the martensite start temperature. Though martensite layer was observed for 309LSS, IN 182, and IN 82 buttering material, martensite was formed at the lowest temperature for IN 82 with respect to the other two alloys. This phenomenon influenced the reduction in width of the martensitic zone for IN 82 buttering material.^[4,39]

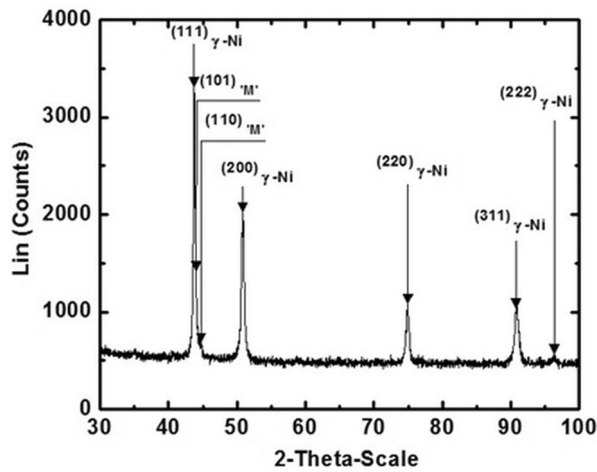


Fig.11—Characteristic X-ray spectrum close to the fusion boundary of LAS-IN 82 (reprinted from Ref. [22]).

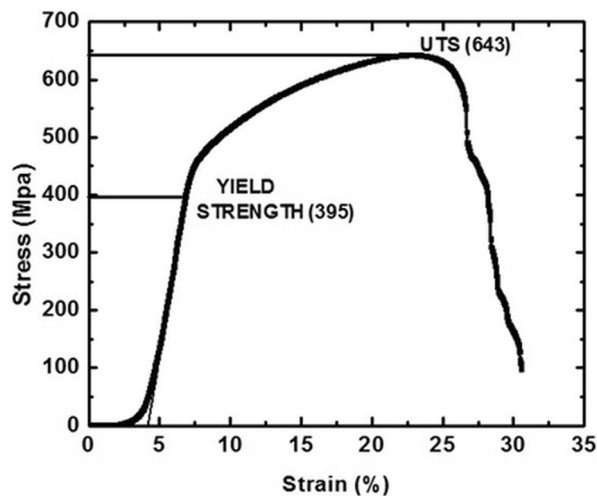


Fig. 12—Engineering stress-strain curve of welded assembly obtained during *in-situ* deformation test.

The microstructure at the interface between buttering material IN 82 and filler metal IN 182 (location E of Figure 1(b)) is revealed in Figure 9(a). It contains columnar crystals on both sides of the interface. Columnar crystals with the transverse directionality of buttering material (Figure 6(a)) and columnar crystals with the longitudinal directionality of filler metal were connected through an unmixed fusion zone (Figure 6(b)). This unmixed zone was developed when the melting points of the two alloys were close to each other.^[4,7] The boundary between the buttering material and filler metal indicated limited mixing within the two alloys. This unmixed zone formation was the result of the restricted extent of substrate melting, followed by resolidification with least dilution.^[6,7,40,41]

Figure 9(b) shows the microstructure at the interface between IN 182 filler metal and 304LN SS base metal (location G of Figure 1(b)). This fusion boundary was nearly straight with epitaxial and superficial grain growth within IN 182 and 304LN SS, respectively. At

this interface, the unmixed zone was predominantly identified with a width of ~ 21 to $25 \mu\text{m}$ due to the limited compatibility of IN 182 with 304LN SS.^[22] Along the fusion boundary of the 304LN SS side, the discontinuous polygonal region existed in the form of laminar layers constituting columnar austenitic grains. Apart from the restricted substrate melting and resolidification effects, the formation of the polygonal region might be owing to the different melting points as well as the elemental migration between IN 182 filler metal and 304LN SS base metal.^[6]

C. Microhardness Distribution

Microhardness distributions across the fusion boundaries of LAS-IN 82 and IN 182-304LN SS interfaces of the DMW joint are shown in Figures 10(a) and (b), respectively. Due to the different phase evolution at different locations during welding and PWHT, the DMW joint exhibited variation in the microhardness profile. A microhardness peak was observed near the interface between the low-alloy steel and buttering material, which was much higher than that of the parent metals (Figure 10(a)). The peak hardness was ~ 348 VHN and was the contribution of martensite.^[4] Immediately after the peak, a decrease in microhardness was observed within the low-alloy steel side, due to the presence of L2 and L3 regions (Figure 7(a)). The microhardness of region L3 was low due to the softening effect.^[42] However, because of its extremely small width, the value could not be precisely measured. The average microhardness of region L2 of low-alloy steel was ~ 265 VHN. Along the low-alloy steel side, microhardness showed fluctuations due to mixed microstructure, which was followed by an increment to reach ultimately a steady value within the base material.

Within buttering material, there was a decrement in the microhardness after the peak, indicating softening. The average microhardness of IN 82 was ~ 250 VHN. Within IN 182, a slight upward trend was found. The microhardness profile near the interface between IN 182 and 304LN SS is shown in Figure 10(b). A decrement in the hardness (~ 230 VHN) was observed close to the fusion boundary of the 304LN SS side owing to the presence of polygonal regions across the interface (Figure 9(b)). The microhardness profile within IN 82, IN 182, and 304LN SS followed a steady state as the phase transformation was absent during welding and PWHT.^[5]

D. XRD Analysis

The characteristic X-ray spectrum of the area near the fusion boundary of low-alloy steel and buttering material is shown in Figure 11. Apart from the γ phase of Ni alloy (IN 82), the X-ray spectrum confirmed the formation of martensite within the IN 82 buttering material. The minute spikes in the spectrum could be attributed to the small phase fraction of martensite with respect to the bulk austenite of IN 82. Other complex alloy/iron carbides might be present within the diffusion zone; however, they could not be identified because of

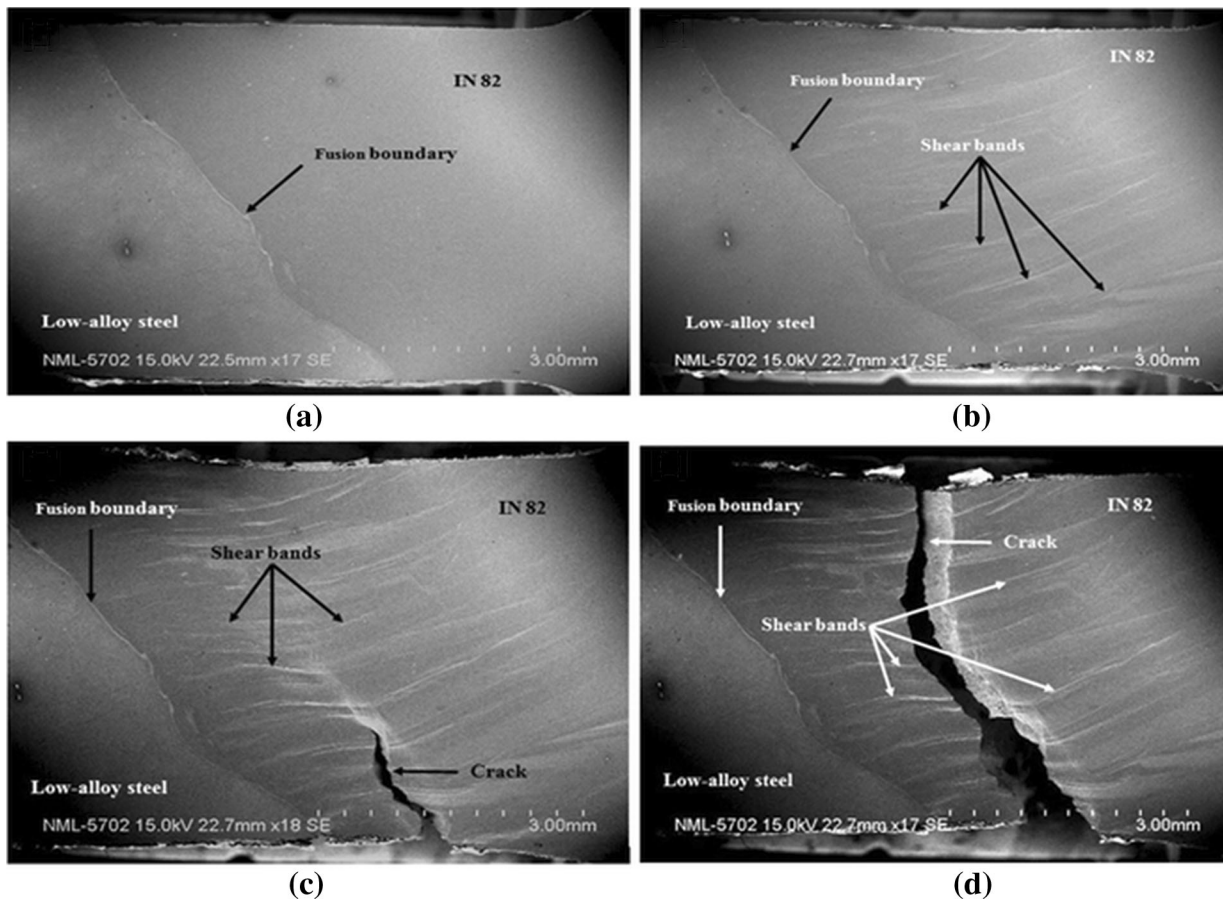


Fig. 13—SEM-SE images during *in-situ* deformation of welded specimen showing (a) structure before YS, (b) appearance of the shear band after YS, (c) fracture initiation, and (d) crack propagation during the test.

their small volume fraction and nanoscale size adjacent to the fusion boundary.^[23]

E. Mechanical Testing

In-situ tensile testing was carried out for the DMW joint. The gage length was ~ 8 mm with the interface between the low-alloy steel and IN 82 at the center (Figure 2(b)). The left part of the gage length consisted of L3, L2, and partially L1 regions of low-alloy steel (Figure 7(a)). The right half contained buttering material (IN 82) with a small extent of filler metal (IN 182), as shown in Figure 2(b). A representative engineering stress-strain curve of welded assembly is shown in Figure 12. The initial stage of the graph is flat (~ 3 pct strain) owing to the grip adjustment during testing. The YS and UTS were found to be 420 ± 5 MPa and 655 ± 12 MPa, respectively. The ductility of the welded joint was $\sim 19 \pm 1$ pct.

During deformation, images were captured at regular intervals to explore various structural changes over gage length (Figure 13). Deformation was absent in the LAS side as the average hardness of the region was comparatively higher than that of the buttering material. Shear bands appeared within the buttering material after the flow curve crossed the yield stress (Figures 13(a) and

(b)). The overlapping of stacking faults in closely packed planes during deformation resulted in the formation of collective planar defects such as shear bands in austenite.^[43] The orientation of shear bands was parallel to the loading axis close to the fusion boundary (Figure 13(b)); however, it changed from grain to grain away from the fusion boundary (Figure 14(a)). The density of shear bands was increased with the increment in applied load (Figure 13(c)), and near UTS, intersecting shear bands were identified (Figure 13(c)). After necking, crack initiated from the edge of the gage section (Figure 13(c)). Subsequently, it moved parallel to the fusion boundary, leading to failure (Figure 13(d)). Thus, failure occurred through the buttering material, which was the weakest zone with minimum microhardness.

Crack propagation was at a distance of ~ 2.2 to 3.0 mm from the interface between low-alloy steel and IN 82. This distance was governed by the diffusional distance of alloying elements from LAS to IN 82. For the same parent alloys, when 309L SS was used as the buttering material, the YS and UTS were 418 ± 4 MPa and 643 ± 12 MPa, respectively.^[22] For a change in buttering alloy to IN 182, the YS and UTS became 379 ± 8 MPa and 584 ± 10 MPa, respectively.^[22] The ductility was reported as 16 ± 1 pct and 17 ± 1 pct, respectively, for two different joints.^[22] In this context,

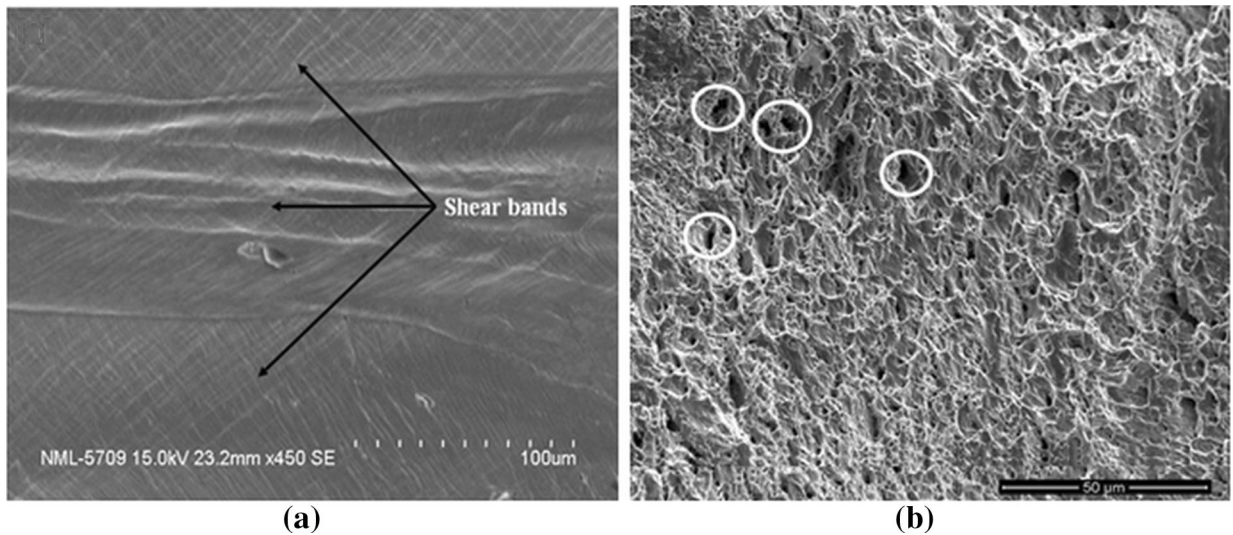


Fig. 14—SEM micrographs showing (a) shear bands of different orientation and (b) fractograph of *in-situ* tested welded joint.

the use of IN 82 buttering material showed an increment in YS, UTS, and ductility for the DMW joint with the same base materials. The high strength of DMW joints with the use of IN 82 buttering material could be attributed to (1) the inherent high strength of IN 82,^[44] (2) the small width of martensite, (3) the high strength of HAZs owing to low heat input in the GTAW process, and (4) the trivial width of the unmixed zones.^[7,28,45]

The fracture surface of the failed samples exhibited ductile fracture through microvoid coalescence (Figure 14(b)). Fractographs of the surface revealed dendritic morphology with microvoids aligned along the primary dendrites. Further, the fractographs exhibited dark irregularly shaped encircled regions (Figure 14(b)). This indicated interdendritic coring, which occurred during welding and contributed to microvoid initiation during *in-situ* deformation test. The aspect ratio of dimples was nearly uniform (~ 1.8).

F. Thermomechanical Simulation

The thermomechanical simulation was carried out to study the behavior of the DMW joint during the real-time service condition in a nuclear power plant, which operated at a temperature of ~ 561 K (288 °C).^[32] The model was simulated using the equations and boundary conditions, as mentioned previously. Temperature-dependent properties of materials were incorporated during analysis. The mesh structure of the DMW joint consisted of 693,516 hexahedral mesh elements, which was a typical average of 16 cell faces. The geometry and mesh structure of the DMW joint are shown in Figures 15(a) and (b), respectively.

G. Temperature and Thermal Stress Distribution

The computed temperature distribution of the DMW joint along the radial direction is shown in Figure 16(a). It can be observed that the maximum temperature of ~ 561 K (288 °C) was in the buttering material IN 82

and the HAZ of the low-alloy steel. The modes of heat transfer from steam that flowed inside the DMW pipe to its adjacent materials were conduction and convection. Different mechanical and temperature-dependent properties (Table II and Figure 4) of materials contributed to developing temperature contour along the radial axis of the assembly. The temperature-dependent properties of individual material and contacts (solid-to-solid bonding based on the welding condition) between the materials controlled the dissipation of heat. It can be identified that the heat dissipation along 304LN SS from the buttering material was minimum. This can be endorsed with the negligible structural changes at the same region (Figure 9). The temperature was found to be minimum (~ 285.26 °C) near IN 182 along 304LN SS. This observation indicated that the temperature dissipation through IN 182 was smaller, thus envisaged better structural stability of IN 182 in comparison to 309L SS during service exploitation.^[46]

The thermostructural analysis of the DMW joint was carried out by importing the temperature mapping to the static structural analysis, taking into account the residual stress within the DMW joint.^[47] The equivalent stress distribution (von Mises) for the DMW joint was portrayed in Figure 16(b). Equivalent stress was found to be equally dispersed at the interface between low-alloy steel and IN 82. The maximum stress was found to be ~ 54.6 MPa, and the thermal stress was shifted and distributed along the filler metal IN 182 (Figure 16(b)).

Generally, the creep stresses along the grain boundaries occur due to residual stress, thermal stresses, and stress owing to the coefficient of thermal expansion (CTE) mismatch between the HAZ and weld metal.^[4,48–50] For a temperature range of 293 K to 873 K (20 °C to 600 °C), the CTEs for low-alloy steel and 304LN SS are ~ 7.5 to 8 $\mu\text{in./in./K}$ and ~9.5 to 10 $\mu\text{in./in./K}$, respectively. Therefore, the difference in CTE resulted in large local stresses in the DMW joint when it was heated to an elevated temperature during service. The low CTE of low-alloy steel tried to keep 304LN SS

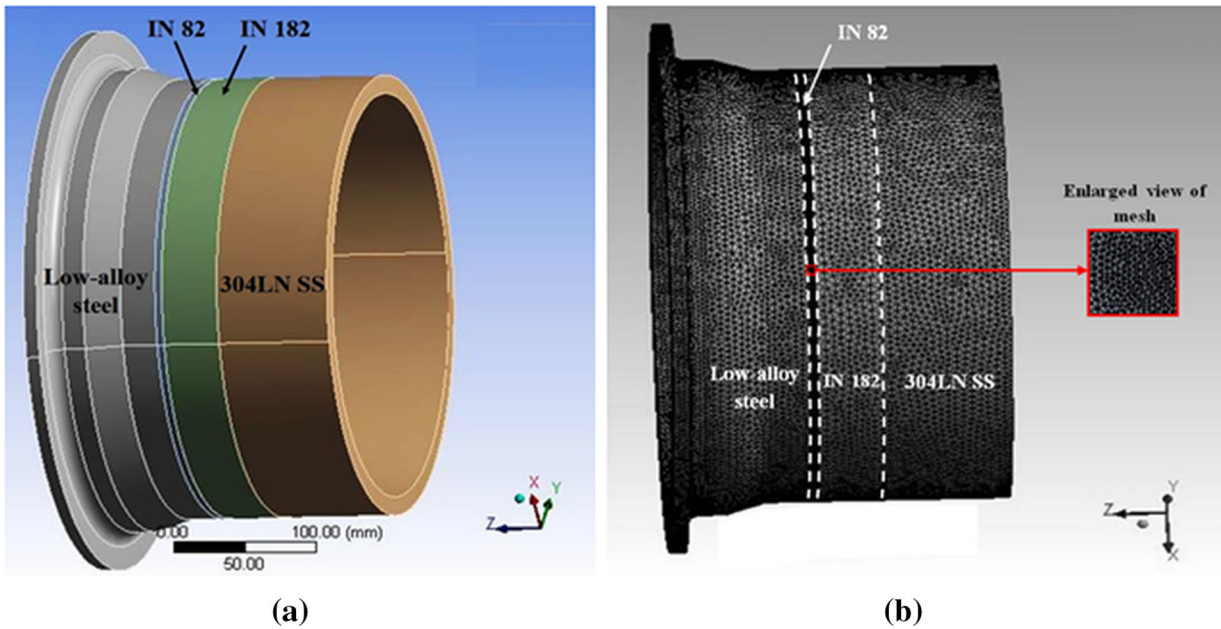


Fig. 15—DMW joint exhibiting (a) geometry and (b) mesh structure.

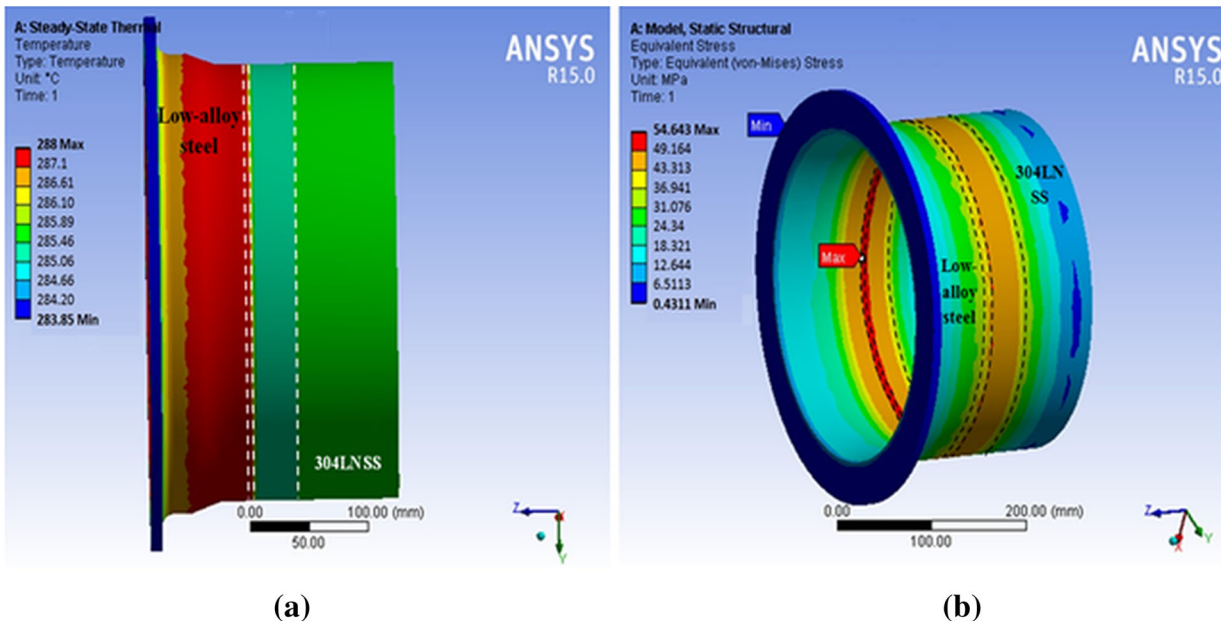


Fig. 16—Simulation results of DMW joint showing the (a) computed temperature profile and (b) thermal stress distribution.

from expanding. Thus, high local stress at the interface between low-alloy steel and IN 82 was produced. However, the CTE of Ni-base alloy (IN 82 and IN 182) is $\sim 8 \mu\text{in./in./K}$, which is close to that of low-alloy steel. Hence, the use of Ni-base alloys protected the weaker HAZ of low-alloy steel by reducing the stress concentration and shifted most of the stress to the HAZ of 304LN SS. The HAZ of 304LN SS was strong enough and crack resistant. This could be endorsed by the microstructural evidence and microhardness investigation. The stress became distributed, leading to a less equivalent stress level at the buttering material and filler

metal. The maximum stress was reduced with the use of IN 82 in comparison to 309L ($\sim 56.2 \text{ MPa}$) and IN 182 ($\sim 55.7 \text{ MPa}$).^[31] This was validated experimentally through an *in-situ* deformation test, where improved strength was obtained with the use of IN 82 buttering material compared to 309L and IN 182.^[22]

During simulation, it was identified that the computational time was increased for thermomechanical analysis (Figure 16(b)) compared to steady-state thermal analysis (Figure 16(a)), as it involved both temperature-dependent structural and thermal properties of the alloys. Though IN 82 buttering material exhibited

satisfactory temperature-dependent mechanical properties compared to 309L and IN 182, the variation/increase in the computational time was found to be minimal during analysis. Improved assumptions may result in further refinement of computational results; however, the present analysis fairly demonstrated stress distribution and its subsequent effects in identifying the weakest region across the DMW joint.

V. CONCLUSIONS

The DMW joint was produced between low-alloy steel and 304LN stainless steel using IN 82 buttering material and IN 182 filler metal. Microstructural examination, microhardness testing, XRD analysis, and *in-situ* tensile testing were carried out for the joints. A 3-D thermomechanical simulation was also done for the DMW joint considering temperature-dependent properties of the materials. It helped in predicting the stress distribution during service. The major observations are summarized as follows.

1. Across fusion boundaries, the microstructure was heterogeneous. Type-I boundary was formed due to columnar grain growth of low-alloy steel within the buttering material. Discontinuous type-II boundary appeared owing to the difference in the crystal structure of two components and heterogeneous nucleation of one of the phases during cooling. Carbon migration from low-alloy steel to buttering material during high-temperature exposure and subsequent cooling resulted in the formation of lath martensite. An unmixed zone occurred across the buttering-filler material and filler material-304LN SS interfaces because of restricted melting of substrates. Epitaxial grain growth was observed near the interface between IN 182 and 304LN SS. Considerable reduction in the width of martensite was found with the use of IN 82 compared to that of 309L and IN 182 buttering materials.
2. Peak hardness was obtained in the martensitic region. Adjacent to peak hardness, there was a sharp drop of the same in LAS and buttering material. Near the fusion boundary between IN 182 and 304LN SS, the reduction in hardness might be attributed to the growth of polygonal grains.
3. During service exposure, the heat was transferred predominantly through the interface between low-alloy steel and IN 82 by conduction and convection. The critical area of thermal stress concentration was within IN 82. Use of IN 82 significantly reduced and shifted the abrupt stress change near the fusion boundary of low-alloy steel and buttering material.
4. The *in-situ* deformation test of a specimen containing a fusion boundary between LAS-IN 82 exhibited adequate strength owing to the low width of martensite, substantial extent of solid solution hardening of buttering material, and reduction in stress gradient. Therefore, in this respect,

considering both experimental and numerical analyses, IN 82 becomes a preferable buttering material compared to 309L SS and IN 182 for joining low-alloy steel and 304LN stainless steel.

REFERENCES

1. C. Jang, J. Lee, J.S. Kim, and T.E. Jin: *Int. J. Press. Vess. Pip.*, 2008, vol. 85, pp. 635–46.
2. R. Chhibber, N. Arora, S.R. Gupta, and B.K. Dutta: *J. Mech. Eng. Sci.*, 2006, vol. 220, pp. 1121–33.
3. R. Miteva and N.G. Taylor: *NESC Report*, Institute for Energy, Netherlands, 2006.
4. J.N. DuPont, J.N. Lippold, and S.D. Kiser: *Welding Metallurgy and Weldability of Ni-Base Alloys*, Wiley, Hoboken, NJ, 2009, pp. 327–76.
5. A. Celik and A. Alasaran: *Mater. Charact.*, 1999, vol. 43, pp. 311–18.
6. H. Naffakh, M. Shamanian, and F. Ashrafizadeh: *J. Mater. Process. Technol.*, 2009, vol. 209, pp. 3628–39.
7. M. Sireesha, S.K. Albert, V. Shankar, and S. Sundaresan: *J. Nucl. Mater.*, 2000, vol. 279, pp. 65–76.
8. J.W. Kim, K. Lee, J.S. Kim, and T.S. Byun: *J. Nucl. Mater.*, 2009, vol. 384, pp. 212–21.
9. H.T. Wang, G.Z. Wang, F.Z. Xuan, C.J. Liu, and S.T. Tu: *Mater. Sci. Eng. A*, 2013, vol. 568, pp. 108–17.
10. D.N. French: *Weld Des. Fab.*, 1981, vol. 54, pp. 92–93.
11. C.D. Lundin: *Weld. J.*, 1982, vol. 61, pp. 58–63.
12. D.W. Wilson: *Weld. J.*, 1990, vol. 69, pp. 71–72.
13. A.K. Bhaduri, S. Venkadesan, P. Rodriguez, and P.G. Mukunda: *Int. J. Press. Vess. Pip.*, 1994, vol. 58, pp. 251–65.
14. N. Taylor, C. Faigy, and P. Gilles: *Assessment of Dissimilar Weld Integrity: Final Report of the NESC-III Project*, Institute for Energy, European Commission, DG-Joint Research Centre, 2006.
15. A. Wiltner, C. Linsmeier, and T. Jacob: *J. Chem. Phys.*, 2008, vol. 129, pp. 084704–1–10.
16. G. Ramamurthy: *Applied Finite Element Analysis*, IK International Publishing House, New Delhi, 2012.
17. T.R. Chandrupatla and A.D. Belegundu: *Introduction to Finite Elements in Engineering*, PHI Learning Pvt. Limited, New Delhi, 2011.
18. J. Goldak, A. Chakravarti, and M. Bibby: *Metall. Trans. B*, 1984, vol. 15B, pp. 299–305.
19. S. Akella, B.R. Kumar, and V. Harinadh: in *1st Int. Conf. on Structural Integrity (ICONS 2014)*, Kalpakkam, India, 2014, p. 141.
20. S. Sahin, M. Toparli, I. Ozdemir, and S. Sasaki: *J. Mater. Proc. Technol.*, 2003, vol. 132, pp. 235–41.
21. S. Xu: *Proc. Eng.*, 2011, vol. 15, pp. 3860–64.
22. M. Ghosh, R. Santosh, S.K. Das, G. Das, B. Mahato, J. Korody, S. Kumar, and P.K. Singh: *Metall. Mater. Trans. A*, 2015, vol. 46A, pp. 3555–68.
23. R. Nivas, G. Das, S.K. Das, B. Mahato, S. Kumar, K. Shivaprasad, P.K. Singh, and M. Ghosh: *Metall. Mater. Trans. A*, 2017, vol. 48A, pp. 230–45.
24. A. Joseph, S.K. Rai, T. Jayakumar, and N. Murugan: *Int. J. Press. Vess. Pip.*, 2005, vol. 82, pp. 700–05.
25. H.P. Seifert and S. Ritter: *J. Nucl. Mater.*, 2008, vol. 378, pp. 197–210.
26. T.K. Yeh, G.R. Huang, M.Y. Wang, and C.H. Tsai: *Progr. Nucl. Energy*, 2013, vol. 63, pp. 7–11.
27. T. Sarikka, M. Ahonen, R. Mougnot, P. Nevasmaa, P. Karjalainen-Roikonen, U. Ehrnsten, and H. Hänninen: *Int. J. Press. Vess. Pip.*, 2016, vol. 145, pp. 13–22.
28. K. Sharma, H.K. Khandelwal, V. Bhasin, and R. Chhibber: *Adv. Mater. Res.*, 2012, vol. 585, pp. 342–46.
29. https://inis.iaea.org/search/search.aspx?orig_q=RN:43001715.
30. D.W. Rathod, S. Pandey, P.K. Singh, and R. Prasad: *Mater. Sci. Eng. A*, 2015, vol. 639, pp. 259–68.

31. R. Santosh, S.K. Das, G. Das, J. Korody, S. Kumar, P.K. Singh, and M. Ghosh: *Metall. Mater. Trans. A*, 2016, vol. 47A, pp. 3511–21.
32. K. Ikushima, A. Takeuchi, T. Okada, S. Itoh, S. Nishikawa, and M. Shibahara: *Proc. 1st Int. Joint Symp. on Joining and Welding*, 1st ed., Hidetoshi Woodhead Publishing, Cambridge, U.K., 2013, pp. 537–45.
33. A. Maekawa, A. Kawahara, H. Serizawa, and H. Murakawa: *J. Press. Vess. Technol.*, 2016, vol. 138, pp. 021401–1–11.
34. F.W. Brust, Y.P. Yang, and P.M. Scott: *Evaluation of Reactor Pressure Vessel (RPV) Nozzle to Hot-Leg Piping Bimetallic Weld Joint Integrity for the VC Summer Nuclear Power Plant*, Contract Number–NRC-04-97-052, Job Code W 6775.
35. S. Nadimi, R.J. Khoushemehr, B. Rohani, and A. Mostafapour: *J. Appl. Sci.*, 2008, vol. 8, pp. 1014–20.
36. H.S. Hosseini, M. Shamanian, and A. Kermanpur: *Mater. Charact.*, 2011, vol. 62, pp. 425–31.
37. F. Matsuda and H. Nakagawa: *Trans. JWRI*, 1984, vol. 13, pp. 159–61.
38. A. Vasilyev: *Materials Science & Technology 2007*, Detroit, MI, Sept. 16–20, 2007; *Fundamentals & Characterization: Phase Stability, Diffusion and Their Application*, organized by J. Morral, Z.K. Liu, R. Arroyave, S.A. Attanasio, N. Sandberg, and Y. Sohn, https://www.academia.edu/6752185/Carbon_Diffusion_Coefficient_in_Complexly_Alloyed_Austenite.
39. M. Pett: *Mater. Sci. Technol.*, 2014, vol. 31, pp. 1370–75.
40. M.D. Rowe, T.W. Nelson, and J.C. Lippold: *Weld. J.*, 1999, vol. 78, pp. 31s–37s.
41. J.N. DuPont and C.S. Kusko: *Weld. J.*, 2007, vol. 86, pp. 51s–54s.
42. M.W.A. Rashid, M. Gakim, Z.M. Rosli, and M.A. Azam: *Int. J. Electrochem. Sci.*, 2012, vol. 7, pp. 9465–77.
43. G.D. Huang, D.K. Matlock, and G. Krauss: *Metall. Mater. Trans. A*, 1989, vol. 20A, pp. 1239–46.
44. www.aircraftmaterials.com/data/weld/.
45. L. Yang, X. Dang, M. Li, and N. Ji: *2nd Int. Conf. on Electronic & Mechanical Engineering and Information Technology (EMEIT-2012)*, Shenyang, China, Sept. 7–9, 2012.
46. J.A. Lichtenfeld, C.J. Tyne, and M.C. Mataya: *Metall. Mater. Trans. A*, 2006, vol. 37A, pp. 147–61.
47. V. Deaconu: *5th Int. Conf. Structural Integrity of Weld Structures (ISCS2007)*, 2007, pp. 20–21.
48. R.L. Klueh and J.F. King: *Weld. J.*, 1982, vol. 61, pp. 302–11.
49. K. Laha, K.S. Chandravathi, K.B.S. Rao, S.L. Mannan, and D.H. Sastry: *Metall. Mater. Trans. A*, 2001, vol. 32A, pp. 115–24.
50. D.J. Kotecki and V.B. Rajan: *Weld. J.-Inc. Weld. Res. Suppl.*, 1997, vol. 76, pp. 57s–66s.